Inorganic Chemistry
Article

Inorg. Chem. **2009,** *48,* 4763–4767 **4763**
DOI:10.1021/ic8022024

Rates of Electron Self-Exchange Reactions between Oxo-Centered Ruthenium Clusters Are Determined by Orbital Overlap

John C. Goeltz, Christina J. Hanson, and Clifford P. Kubiak*

Department of Chemistry and Biochemistry, University of California San Diego, 9500 Gilman Drive, M/C 0358, La Jolla, California 92093-0358

Received November 17, 2008

We report rate constants for electron self-exchange of trinuclear ruthenium clusters of the type $[Ru_3O(OAc)_6(CO)(L)_2]^{0/-}$, where L is 4-cyanopyridine, pyridine, or 4-(dimethylamino)pyridine. Rate constants were determined by ^1H NMR line-broadening experiments in CD_3CN, CD_2Cl_2, and THF-d_8, and range from 6.5×10^6 to 2.5×10^8 s^{-1} M^{-1}. Faster self-exchange is observed with more electron-withdrawing substituents on the ancillary pyridine ligands. This effect is attributed to increased orbital overlap between the donor and acceptor as more electron density is drawn onto the pyridine ring. This view is supported by measured NMR contact shifts of the pyridyl protons which reflect increased electron spin density with increasing pyridine ligand electron-withdrawing ability. Normal solvent dependence is also observed, where higher outer-sphere reorganization energies lead to slower exchange.

Introduction

Electron self-exchange is one of the simplest chemical reactions, but also one of the most revealing. Within the context of the Marcus−Hush theory of electron transfer[1,2] (ET), rates of electron self-exchange can be related directly to the total reorganization energy for ET, λ, and by the Marcus cross relation, to rates of intermolecular ET with other redox agents.[3,4] The mixed valence states of the "dimer-of-trimer" complexes of the general type $[Ru_3O(OAc)_6(L)(CO)(\mu\text{-BL})Ru_3O(OAc)_6(L)(CO)]^-$ (where BL = bridging ligand) have been the subject of considerable study.[5−9] Several aspects of the ET chemistry of these mixed valence ions, notably ET rates on the vibrational time scale that give rise to coalescence of infrared (IR) spectral line shapes,[5,6] dependence of ground-state ET rates on solvent dynamics,[7,10] appearance of only totally symmetric bridging ligand modes of vibration in the resonance Raman spectra measured within the intervalence charge transfer bands,[11] and non-Arrhenius kinetic behavior in freezing solvents,[7] challenge normal two-state ET theoretical models. Here, we examine the self-exchange ET reactions of ruthenium clusters of the type $[Ru_3O(OAc)_6(CO)(L)_2]$ (Figure 1) which constitute "half" of the dimer-of-trimer mixed valence ions. The three different ancillary pyridine ligands used dictate the redox potentials of the clusters, as shown in Figure 2. Our intent is to determine the rates of self-exchange, individual cluster reorganization energies, and general features that will shed light on the unusual intramolecular ET properties of the pyrazine-bridged mixed valence ions that are based on the isostructural redox unit.

Experimental Section

Preparation and Purification of Chemicals. The complexes **1**, $Ru_3O(OAc)_6(CO)(cpy)_2$; **2**, $Ru_3O(OAc)_6(CO)(py)_2$; and **3**, $Ru_3O(OAc)_6(CO)(dmap)_2$, were isolated as byproducts during previously reported preparations.[12] CD_3CN (D, 99.8%) and CD_2Cl_2 (D, 99.9%) were obtained from Cambridge Isotope Laboratories (CIL) and distilled under argon from calcium hydride before use. THF-d_8 (D, 99.5%) was obtained from

*To whom correspondence should be addressed. E-mail: ckubiak@ucsd.edu.

(1) Hush, N. S. *Prog. Inorg. Chem.* **1967**, *8*, 391.
(2) Marcus, R. A. *Annu. Rev. Phys. Chem.* **1964**, *15*, 155.
(3) Stanbury, D. M. *Nucl. Factors Main-Group Electron Transfer Reactions* **1997**, *253*, 165–182.
(4) Nelsen, S. F.; Ismagilov, R. F.; Gentile, K. E.; Nagy, M. A.; Tran, H. Q.; Qu, Q. L.; Halfen, D. T.; Odegard, A. L.; Pladziewicz, J. R. *J. Am. Chem. Soc.* **1998**, *120*(32), 8230–8240.
(5) Ito, T.; Hamaguchi, T.; Nagino, H.; Yamaguchi, T.; Kido, H.; Zavarine, I. S.; Richmond, T.; Washington, J.; Kubiak, C. P. *J. Am. Chem. Soc.* **1999**, *121*(19), 4625–4632.
(6) Ito, T.; Hamaguchi, T.; Nagino, H.; Yamaguchi, T.; Washington, J.; Kubiak, C. P. *Science (USA)* **1997**, *277*(5326), 660–663.
(7) Lear, B. J.; Glover, S. D.; Salsman, J. C.; Londergan, C. H.; Kubiak, C. P. *J. Am. Chem. Soc.* **2007**, *129*, 12772–12779.
(8) Londergan, C. H.; Kubiak, C. P. *Chem.—Eur. J.* **2003**, *9*(24), 5962–5969.
(9) Salsman, J. C.; Kubiak, C. P.; Ito, T. *J. Am. Chem. Soc.* **2005**, *127*(8), 2382–2383.
(10) Londergan, C. H.; Salsman, J. C.; Ronco, S.; Dolkas, L. M.; Kubiak, C. P. *J. Am. Chem. Soc.* **2002**, *124*(22), 6236–6237.
(11) Rocha, R. C.; Brown, M. G.; Londergan, C. H.; Salsman, J. C.; Kubiak, C. P.; Shreve, A. P. *J. Phys. Chem. A.* **2005**, *109*(40), 9006–9012.
(12) Ota, K.; Sasaki, H.; Matsui, T.; Hamaguchi, T.; Yamaguchi, T.; Ito, T.; Kido, H.; Kubiak, C. P. *Inorg. Chem.* **1999**, *38*(18), 4070–4078.

© 2009 American Chemical Society
Published on Web 4/16/2009

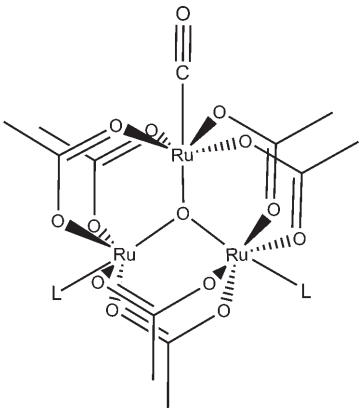

Figure 1. The three clusters used in this study: **1**, L = 4-cyanopyridine (cpy); **2**, L = pyridine (py); and **3**, L = 4-(dimethyl)aminopyridine (dmap).

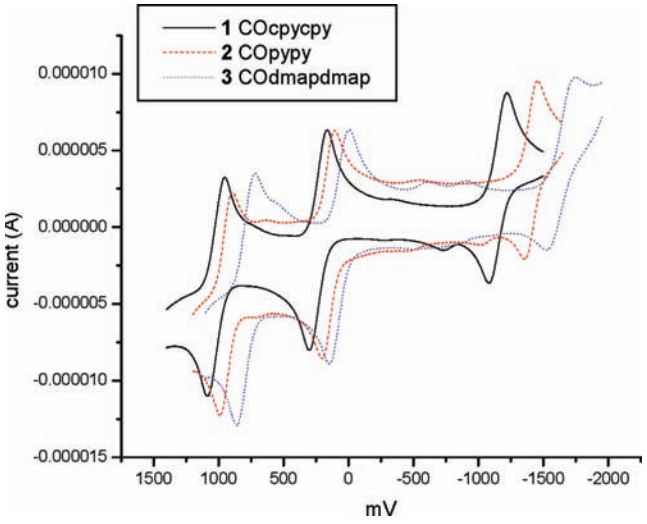

Figure 2. Electrochemistry of ruthenium trimers with different pyridyl ligands in CH_2Cl_2 with 0.1 M TBAH and glassy carbon working, platinum wire counter, and Fc/Fc^+ reference electrodes.

CIL in ampules and used as received. Decamethylcobaltocene was obtained from Aldrich, stored at −20 °C in a glovebox, and used without purification.

Sample Preparation. Samples for NMR and IR experiments were prepared in a nitrogen-filled glovebox. The 7.0 mM solutions were prepared in the appropriate dried deuterated solvent, and approximately half of the solution was added to a small excess (1.2−1.5 equiv) of decamethylcobaltocene. The reduced sample was filtered through glass wool to remove small amounts of impurities from the reductant. The fully oxidized and reduced solutions were mixed in varying proportions to prepare samples for NMR. A total of 0.6 mL was added to either J-Young tubes (800 MHz, Wilmad) or sealed standard tubes (500 MHz, Wilmad), with no difference in the spectra obtained. Samples for IR were injected into liquid IR cells with CaF_2 windows and ∼0.5 mm Teflon spacers and sealed in the glovebox. All samples were analyzed immediately, though CD_3CN and THF solutions were stable for days unless opened to the atmosphere. Singly reduced **3** was unstable in CD_2Cl_2, degrading in less than 1 min.

NMR Data Collection and Analysis. ^1H spectra were collected on a JEOL 500 MHz NMR spectrometer and analyzed using JEOL Delta software. A total of 64 scans of 131 072 data points (0.15 Hz resolution) were collected from +25 to −15 ppm. Peak positions were used to determine the ratio of oxidized to reduced sample after a linear relationship was confirmed by infrared measurements, as described below. Peak widths at half-height were measured in Delta. Each reported rate constant is an average of at least four values calculated from eq 1 below. All spectra were recorded at the ambient temperature of the instrument (18−20 °C).

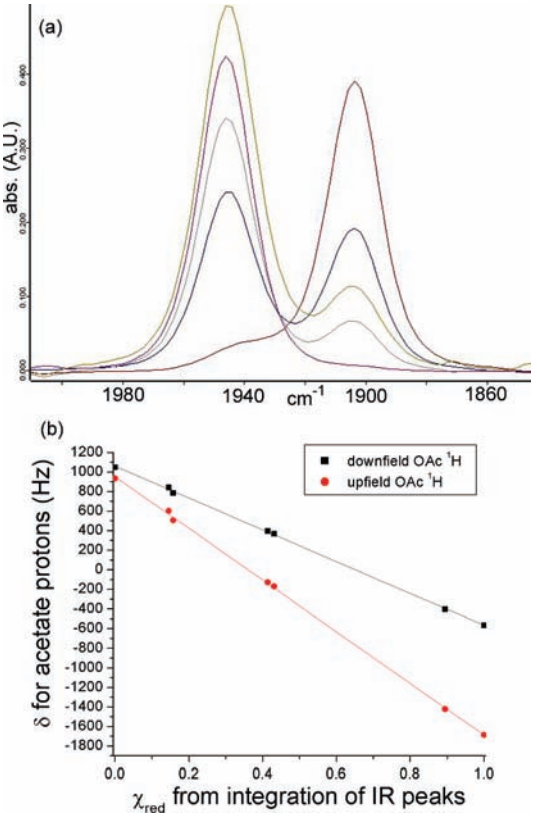

Figure 3. (a) IR spectra of the ν(CO) region for **1** in CD_2Cl_2, with varying mole fractions of [red]/[ox]. (b) Plot of χ_{red} determined from integration of IR peaks vs chemical shift of acetate protons. The linear relationship confirms fast exchange on the NMR time scale.

Infrared Data Collection and Analysis. Infrared spectra were collected on a Bruker Equinox 55 FTIR spectrometer. After solvent subtraction, CO peaks were fit to mixed Gaussian/Lorentzian line shapes using Bruker OPUS software. Suitably enlarged printouts were cut along the peak fit lines and weighed to give ratios of oxidized to reduced species.

Electrochemical Measurements. Electrochemistry was performed on a BAS CV-50W in dried degassed CH_2Cl_2 with 0.1 M tetrabutylammonium hexafluorophosphate (TBAH, recryst. from MeOH and dried under a vacuum at 80 °C) and ∼5 mM sample at a scan rate of 100 mV/s in a dedicated glovebox. The working electrode was a glassy carbon disk (0.3 cm diameter). The counter electrode was a platinum wire, and the reference was ferrocene/ferrocenium.

Results and Discussion

The mole fractions of diamagnetic neutral clusters to paramagnetic singly reduced clusters in solution were initially determined by IR spectroscopy. Spectra for **1** in CD_2Cl_2 are shown in Figure 3a. Ratios were determined by integration of the ν(CO) bands for the neutral cluster (∼1940 cm^{-1}) and the singly reduced cluster (∼1900 cm^{-1}). The ν(CO) region for the mixed solutions was not coalesced and could be fit to two well-resolved peaks, giving an upper bound to k_{ET} of $\sim 10^{10}$ to 10^{11} s^{-1} M^{-1}.[6] The exchange was in the fast regime (where $k(C_{tot}) \gg 2\pi(\Delta\nu)$) on the NMR time scale, as the chemical

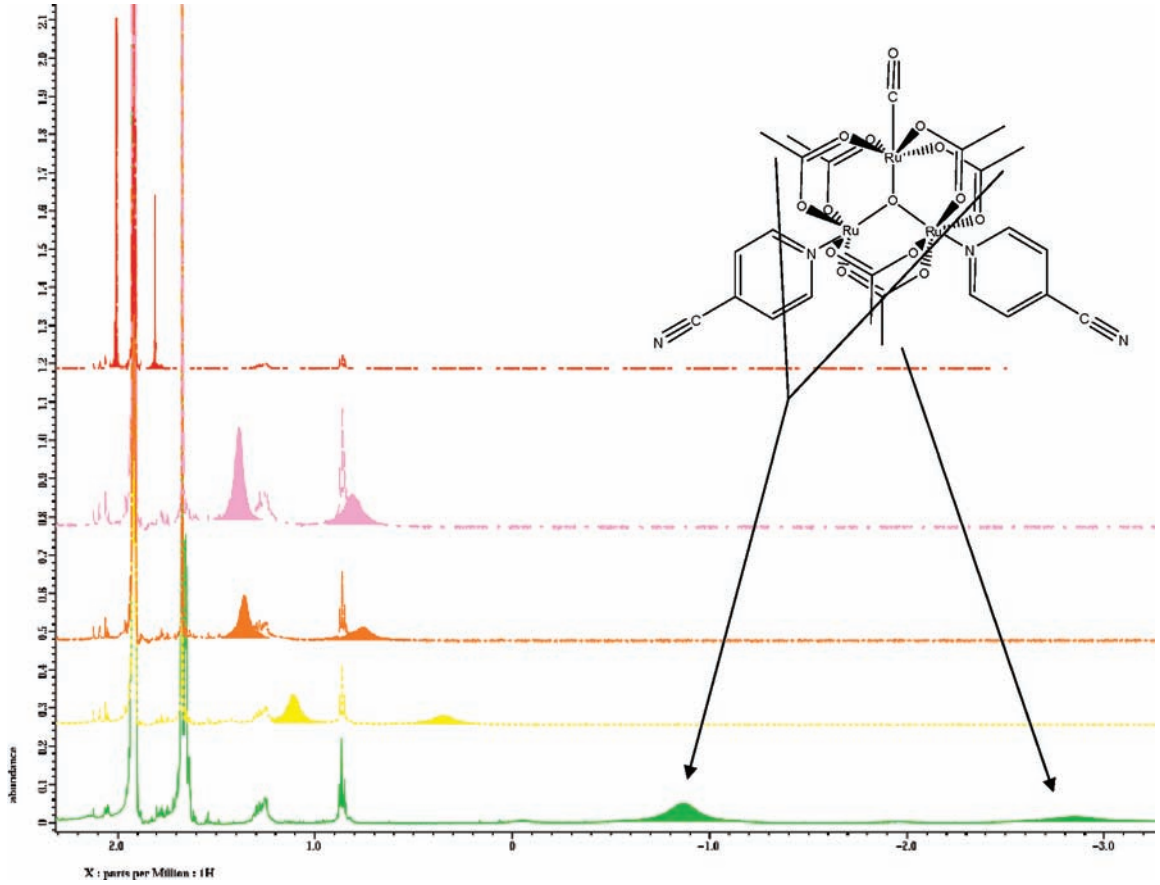

Figure 4. Representative ^{1}H NMR spectra with varying mole fractions of diamagnetic and paramagnetic **1** in CD_3CN.

Table 1. Electron Transfer Rate Constants ($\times 10^7$ s^{-1} M^{-1})

	CD_3CN	THF-d_8	CD_2Cl_2
1 COcpycpy	13	20	30
2 COpypy	1.8	20	7
3 COdmapdmap	0.7	2	

shifts for exchanging species were averages of the diamagnetic and paramagnetic chemical shifts, weighted by their respective mole fractions. This is shown in the linear relationship in the mole fraction of the reduced complex versus the acetate chemical shift in Figure 3b.

Rate constants were determined using the equation

$$k_{ET} = \frac{4\pi\chi_d\chi_p(\Delta\nu)^2}{(W_{dp} - \chi_p W_p - \chi_d W_d)C_{tot}} \quad (1)$$

where χ_d and χ_p are the mole fractions of diamagnetic and paramagnetic species, $\Delta\nu$ is the difference in chemical shift between diamagnetic and paramagnetic species in hertz, W_{dp} is the peak width at half-maximum for the mixture in question, W_d and W_p are the widths for the pure diamagnetic and paramagnetic species, and C_{tot} is the total concentration in moles per liter.[13] Representative NMR spectra for **1** in CD_3CN are shown in Figure 4. The rate constants measured ranged from 10^6 to 10^8 s^{-1} M^{-1} and are shown in Table 1. These rate constants are comparable in magnitude to those found by NMR for many other 0/+ and 0/− couples, though the range is remarkable for analogous self-exchange couples.[14−19] In a particularly relevant study reported by Meyer, $Ru_3O(OAc)_6(py)_3^{0/+}$ exhibited $k_{ET} = 1.1 \times 10^8$ s^{-1} M^{-1} in CD_2Cl_2.

Looking at the observed k_{ET} for complexes **1**−**3**, one trend is immediately clear: more electron-withdrawing substituents on the ancillary pyridine ligands lead to faster self-exchange in all three solvents. We attribute this to increasing donor−acceptor orbital overlap, or "contact area", as more electron density is drawn onto the pyridine ligands of the $[Ru_3O(OAc)_6(CO)(L)_2]^-$ donor.

The increasing effective contact area is also clearly apparent in the increasing paramagnetic contact shift for the pyridyl protons with more electron-withdrawing groups at the pyridine para position. Average $\Delta\delta$'s for pyridyl protons in the three complexes and their reduced counterparts in CD_3CN are shown in Figure 5. As the pyridine ligand becomes less basic (lower pK_a), more electron density is drawn onto the ring in the reduced cluster, and the contact shift is greater.

(13) Chan, M.-S.; DeRoos, J. B.; Wahl, A. C. *J. Phys. Chem.* **1973**, *77*(18), 2163–2165.

(14) Coddington, J.; Wherland, S. *Inorg. Chem.* **1997**, *36*(27), 6235–6237.
(15) Walsh, J. L.; Baumann, J. A.; Meyer, T. J. *Inorg. Chem.* **1980**, *19*(7), 2145–2151.
(16) Nielson, R. M.; Golovin, M. N.; McManis, G. E.; Weaver, M. J. *J. Am. Chem. Soc.* **1988**, *110*(6), 1745–1749.
(17) Nielson, R. M.; McManis, G. E.; Golovin, M. N.; Weaver, M. J. *J. Phys. Chem.* **1988**, *92*(12), 3441–3450.
(18) Kowert, B. A.; Fehr, M. J.; Sheaff, P. J. *Inorg. Chem.* **2008**, *47*(13), 5696–5701.
(19) Yang, E. S.; Chan, M. S.; Wahl, A. C. *J. Phys. Chem.* **1975**, *79*(19), 2049–2052.

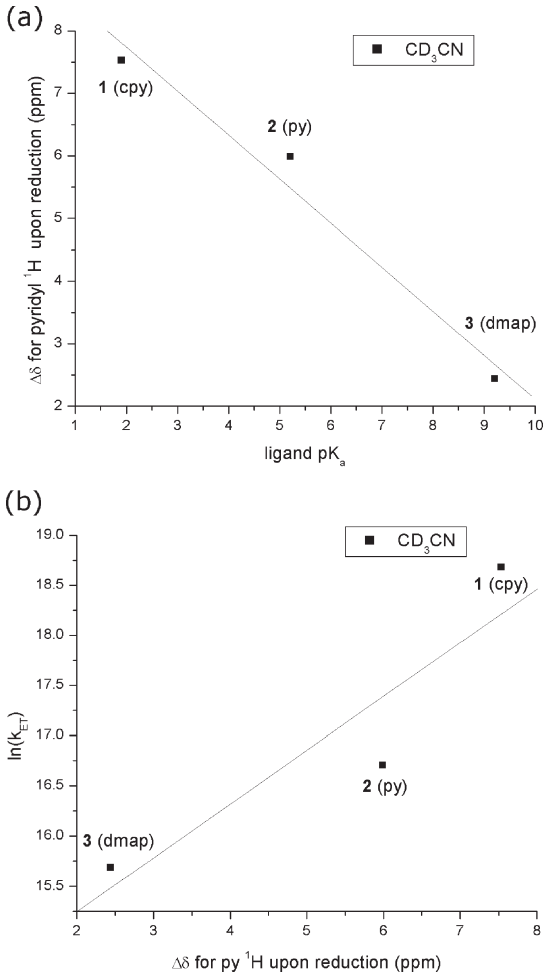

Figure 5. (a) Plot of ligand pK_a vs the average change in chemical shift ($\Delta\delta$) for the pyridyl protons upon reduction of the neutral cluster in CD_3CN. (b) Plot of $\Delta\delta$ vs ln(k_{ET}) illustrating that increased electron density on peripheral ligands corresponds to faster rates of ET.

A logarithmic plot of k_{ET} versus ligand pK_a is linear (Figure 6), suggesting that the electron-withdrawing nature of the ligands and thus the effective contact area factor into the activation energy for ET. To the best of our knowledge, a simple quantitative proxy for orbital overlap has never before been correlated with observed rates of electron self-exchange, though orbital overlap has previously been invoked to explain the difference in self-exchange rate constants for the ferrocene/ferrocenium ($Fc^{0/+}$) and cobaltocene/cobaltocenium ($Cc^{0/+}$) couples.[16] In short, the Fc orbital in question is iron-based, whereas in Cc the orbital is spread over more of the molecule.

It is unlikely that nuclear reorganization factors and inner-shell barriers play large roles in determining the differences in rate constants for **1**−**3**. The shift in the ν(CO) stretching frequency is about the same (~40 cm^{-1}) upon reduction of each cluster, suggesting that the inner-sphere reorganization energies are comparable. We use the shift in ν(CO) here not as a direct marker for low-frequency modes that make up the reorganization barrier but only for what it is: the best infrared probe of electronic redistribution in the cluster. The pre-exponential frequency factor ν_n is not likely important either, as pyridine skeletal modes change by less than 1.5% from 4-cyanopyridine to 4-(dimethylamino)pyridine. Cluster skeletal modes in the vicinity of the point of substitution can be expected to change by no more than this, and a change in the pre-exponential of a few percent cannot explain observed rate constants differing by more than an order of magnitude. Monoanionic pyrazine-bridged dimers of these clusters exhibit picosecond ground-state ET, and the reorganization energy, λ, for the pair of exchanging clusters has been estimated at 1.25 eV, or 10 000 cm^{-1}.[7,20] The intermolecular electron transfer studied here must be in the adiabatic regime with H_{AB} on the order of 10−20% of the reorganization energy, λ, to achieve the observed rates on the order of 10^8 s^{-1}. While low-frequency skeletal modes and local solvent modes are expected to contribute to λ,[21] there is no spectroscopic evidence to support this as the main factor in determining rate constants, nor any reason why these modes should make the barrier for **3** so much larger than for **1** that the k_{ET} is over an

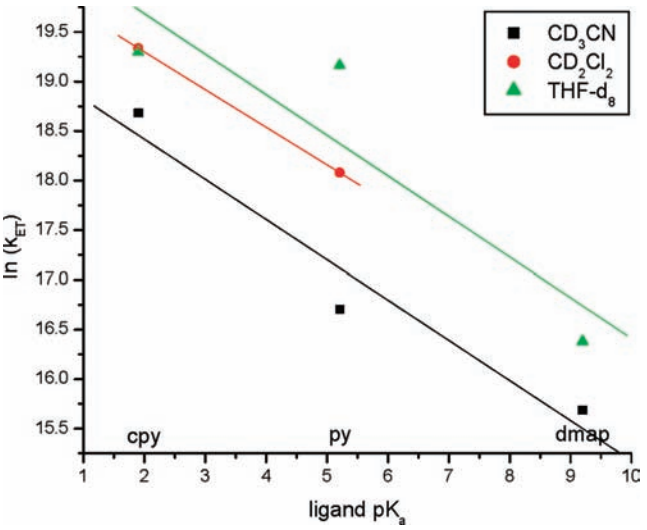

Figure 6. Plot of ln(k_{ET}) vs ligand pK_a with linear fits. The linear relationship indicates that pK_a is a good proxy for the amount of electron density on the pyridine ligand in the reduced state and thus the donor−acceptor orbital overlap, which figures into the activation barrier to ET.

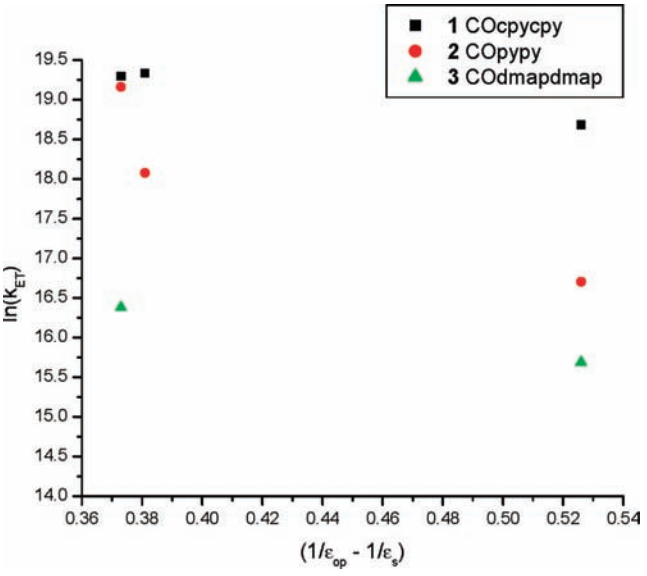

Figure 7. Plot of ln(k_{ET}) vs ($1/\varepsilon_{op} - 1/\varepsilon_s$). The rate decreases with increasing outer-sphere solvent reorganization energy.

(20) Londergan, C. H.; Salsman, J. C.; Lear, B. J.; Kubiak, C. P. *Chem. Phys.* **2006**, *324*(1), 57–62.
(21) Endicott, J. F.; Uddin, M. J. *Coord. Chem. Rev.* **2001**, *219*, 687–712.

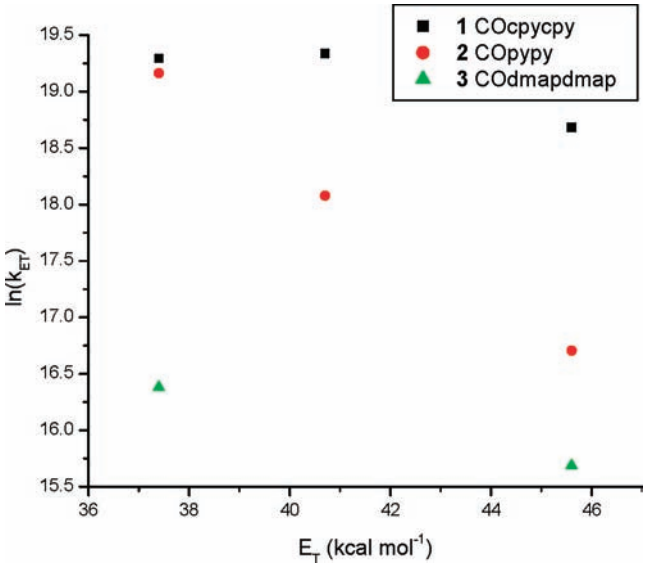

Figure 8. Plot of $\ln(k_{ET})$ vs solvent microscopic polarity.

order of magnitude slower. Essentially, the clear evidence of significant and increasing unpaired electron spin density on the peripheral pyridine ligands of the anions of **1**, **2**, and **3** as the rate of ET increases (Figure 5), combined with the fact that replacing one of the pyridine ligands with a bridging pyrazine produces strongly delocalized mixed valence ions,[5] provides a consistent physical model for explaining rates of ET in both systems.

With respect to outer-sphere thermodynamic solvent parameters, **1**−**3** behave normally. A log plot of k_{ET} versus the solvent variable portion of the outer-sphere reorganization energy[7] $(1/\varepsilon_{op} - 1/\varepsilon_s)$ shows that self-exchange is slower with increasing outer-sphere solvent reorganization energy (Figure 7). The observed rate constants also correlate well with solvent microscopic polarities[7] (Figure 8). Here, the reaction slows with increasing E_T.

Conclusions

The present results add to the quantitative understanding of electron self-exchange reactions. We were able to correlate the electron-withdrawing ability of ancillary ligands to intermolecular electron transfer rate constants. A plot of $\ln(k_{ET})$ versus the pyridine ligand pK_a is linear, suggesting that donor−acceptor orbital overlap is a major contributor to the ET activation barrier. A greater ^{1}H NMR contact shift for the pyridyl protons indicates increased electron density on ancillary pyridine ligands with more electron-withdrawing groups. This leads to an increase in V_{AB}, the matrix element that describes the mixing of the two wave functions involved in electron exchange. The increased overlap decreases the activation energy for electron transfer.

This work also underscores the general importance of metal cluster orbital extension onto ligands. Often, it is assumed that an oxidation state or a redox event is localized on a metal center or cluster. On the contrary, the delocalization of charge onto peripheral ligands is shown in this work to play an important role in ET. The effect here is so strong that, by simple variation of the pyridine ligands, rate constants can be varied by almost 2 orders of magnitude for a reaction with zero thermodynamic driving force.

Finally, the delocalization of the electron density onto the pyridine ligands illustrates how the $[Ru_3O(AcO)_6(CO)(L)_2]$ units contribute to such strongly interacting mixed valence ions when they are bridged by pyrazine.[22] Pyrazine is an even more effective electron-withdrawing pyridyl ligand ($pK \sim 1$) than the three pyridines employed in this study. It would be expected then that delocalization onto the pyrazine bridge would be preferred, promoting electron transfer to the other Ru_3 cluster, and contributing to intercluster electron transfer and delocalization. This also helps explain why the fastest exchange times are observed for dimers with electron-donating and aliphatic nonbridging ancillary ligands, which do not have low-lying π^* orbitals to accept electron density from the reduced cluster in the ancillary positions.[23]

Acknowledgment. We thank Dr. Anthony Mrse in the UCSD NMR facility, Ms. Starla D. Glover, and Dr. Benjamin J. Lear for helpful discussions about synthesis and results, as well as the introduction to this manuscript. We gratefully acknowledge support from NSF CHE-0616279.

(22) Salsman, J. C.; Ronco, S.; Londergan, C. H.; Kubiak, C. P. *Inorg. Chem.* **2006**, *45*, 547–554.
(23) Yamaguchi, T.; Imai, N.; Ito, T.; Kubiak, C. P. *Bull. Chem. Soc. Jpn.* **2000**, *73*(5), 1205–1212.